

Charging and discharging of single conjugated-polymer nanoparticles

RODRIGO E. PALACIOS, FU-REN F. FAN, JOHN K. GREY, JUNGDON SUK, ALLEN J. BARD AND PAUL F. BARBARA*

Department of Chemistry and Biochemistry and the Center for Nano- and Molecular Science and Technology, University of Texas, Austin, Texas 78712, USA

*e-mail: p.barbara@mail.utexas.edu

Published online: 22 July 2007; doi:10.1038/nmat1959

Despite intense, long-term interest in organic semiconductors from both an applied and fundamental perspective, key aspects of the electronic properties of these materials remain poorly defined. A particularly challenging problem is the molecular nature of positive charge carriers, that is, holes or oxidized species in organics. Here, the unique ability of single-molecule spectroelectrochemistry (SMS-EC) to unravel complex electrochemical process in heterogeneous media is used to study the oxidation of nanoparticles of the conjugated polymer poly(9,9-dioctylfluorene-*co*-benzothiadiazole). A reversible hole-injection charging process has been observed that occurs primarily by initial injection of shallow (untrapped) holes, but soon after the injection, a small fraction of the holes becomes deeply trapped. Good agreement between experimental data and simulations strongly supports the presence of deep traps in the studied nanoparticles and highlights the ability of SMS-EC to study energetics and dynamics of deep traps in organic materials at the nanoscale.

Various types of evidence show that in addition to shallow trapped mobile holes in organics, holes can also be deeply trapped^{1–8}. Deeply trapped holes are believed to be responsible for large space charges within the thin layers (10–100 nm) and at the interfaces of a device. This space charge in turn can greatly influence device physics, such as the charge injection current at the anode of a heterolayer diode, the electron/hole pair recombination efficiency in an organic light-emitting diode⁷ and the local electric field in a field-effect transistor^{2–6}.

Most of the published data on deeply trapped holes have been obtained by device studies (for example, current/capacitance–voltage measurements), which often require modelling a complicated device. Herein we investigate charging and discharging processes (that is, redox) by electrochemical methods in which charge injection is controlled by a well-defined potential drop at the electrode–electrolyte interface. Hole injection from an anode of an organic diode, in contrast, is more difficult to control and model, and covers a much smaller effective potential range.

Complications usually seen in the electrochemistry of non-porous polymer films^{9,10} are avoided in this research by investigating the electrochemistry of organic nanoparticles^{11,12} that are immobilized in an ion-conducting Nafion film (Fig. 1a)⁹. The film provides a low-resistance support for the polymer nanoparticles and minimizes the contributions of uncompensated resistance and ion-transport effects in the measurements. This approach is shown herein to lead to good electrical contact of the nanoparticles with the electrode (allowing electron transfer ‘across’ the compact electrical double layer). The specific material we investigate is the conjugated polymer, poly(9,9-dioctylfluorene-*co*-benzothiadiazole) (F8BT; Fig. 1c, left inset), which has promising applications in organic light-emitting diodes and photovoltaic devices, and is known to efficiently trap holes^{1,7,13}.

The main tool in this study is a new indirect electrochemical technique, single-molecule spectroelectrochemistry (SMS-EC),

which allows for ultrasensitive ‘indirect’ electrochemical measurements on the basis of fluorescence quenching on electron transfer of single fluorescent molecules or aggregates, one particle at a time¹⁴ (see the Methods section). The ability to study the fluorescence quenching of individual nanoparticles greatly simplifies the electrochemical data analysis of the faradaic process by removing the interferences from resistance effects, double-layer charging and heterogeneity due to particle size and irreversible electrochemical processes, which are often encountered in conventional electrochemical techniques¹⁰. Recent spectroscopic experiments indicate that the core of the particles is indistinguishable from bulk F8BT, supporting the relevance of this work to the bulk polymer¹¹. This work also builds on previous SMS-EC¹⁴ and SMS^{15–17} studies of the single isolated F8BT molecules.

The bulk electrochemical behaviour of F8BT nanoparticles embedded in a Nafion film is shown in Fig. 1c in the form of a cyclic voltammogram at a scan rate, ν , of 0.1 V s⁻¹. When the potential, E , of the working electrode relative to the reference electrode is scanned anodically (positively) from the initial potential (0 V versus a ferrocene/ferrocenium redox couple (Fc/Fc⁺)), the onset of the oxidation wave is observed near 1.3 V owing to charging of the nanoparticles with positive charges (holes) (that is, oxidation of F8BT). Control measurements of a pure Nafion film (Fig. 1c, right inset) indicate that background currents are negligible over the studied potential range (0–1.6 V versus Fc/Fc⁺). In the reverse scan direction, a broad reduction peak is observed owing to discharging of the nanoparticles (that is, re-reduction of the oxidized F8BT molecules). The cathodic charge collected during the discharge process (that is, reduction) in Fig. 1c is only about 57% of the initially injected anodic charge (that is, oxidation) at this scan rate (see Supplementary Information, Fig. S3). The large shift between the oxidation and reduction wave and the low recovery of charge in the re-reduction is indicative of electrochemically irreversible

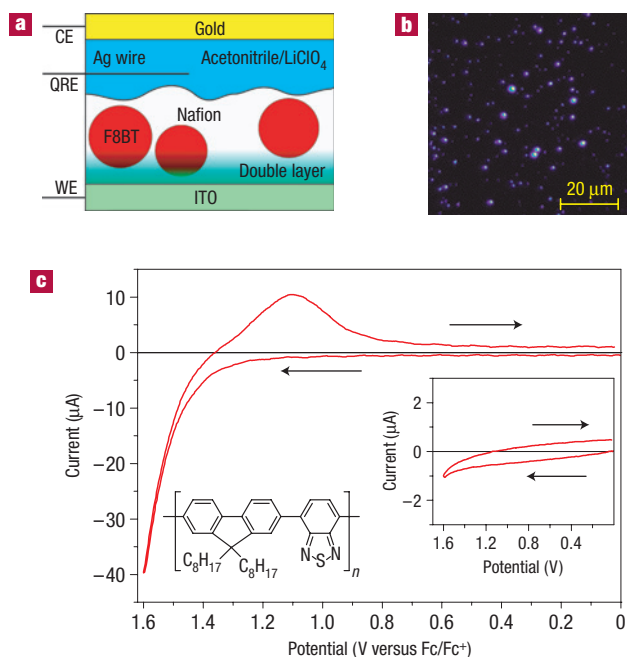


Figure 1 SMS-EC cell configuration and F8BT aggregates bulk electrochemistry. **a**, SMS-EC cell. CE: Counter electrode; QRE: Quasireference electrode; WE: Working electrode. **b**, Wide-field total internal reflectance fluorescence image of an SMS-EC cell. **c**, Cyclic voltammogram of F8BT in Nafion thin film on ITO in 0.2 M LiClO₄/acetoneitrile solution at potential scan rate of 0.1 V s⁻¹. Right inset: Cyclic voltammogram of a Nafion film showing very small background currents over the scanned range. Left inset: F8BT structure.

behaviour. Cyclic voltammograms in the potential ranges of 0–1.8 and 0–1.6 V versus Fc/Fc⁺ show similar reversibility and stability (see Supplementary Information, Fig. S2).

From a semiconductor perspective, electrochemical data reflect the energetics and dynamics of the charging/discharging of the film with holes. Thus, the irreversible behaviour can be ascribed to the deep trapping of holes in the conjugated polymer film. For small molecule systems, irreversible electrochemistry is typically due to following chemical reactions such as H⁺/H transfer, polymerization and isomerization¹⁰. Such effects may be responsible for the irreversible behaviour of the conjugated polymer films, or alternatively, some unknown relaxation of the polymer structure may be also responsible.

A considerably more detailed view of the charging/discharging of F8BT nanoparticles is found in the SMS-EC data in Fig. 2. The electrochemical cells used in these experiments (Fig. 1a) comprised a planar transparent indium tin oxide (ITO) working electrode, a planar gold counter electrode and a silver quasireference electrode (AgQRE) (see the Methods section). Here, the fluorescence intensity (Fig. 2b) of a small number of the investigated individual nanoparticles is plotted as a function of time while linearly scanning the potential (Fig. 2a) of the working electrode in a pristine cell. The individual fluorescence intensity, $I_{fl}(t)$, curves exhibit a large intensity drop assigned to fluorescence quenching due to oxidation of F8BT in the 1–2 V range. In a typical SMS-EC cell, a large fraction of the total number of investigated particles exhibited bias-dependent fluorescence intensity modulation. In the case of these electroactive particles, the shape of their $I_{fl}(t)$ curves reflects the time dependence of the concentration of injected holes, [holes(t)], in the nanoparticle (see below). In the SMS-EC experiment, a much lower concentration of F8BT is used (of the

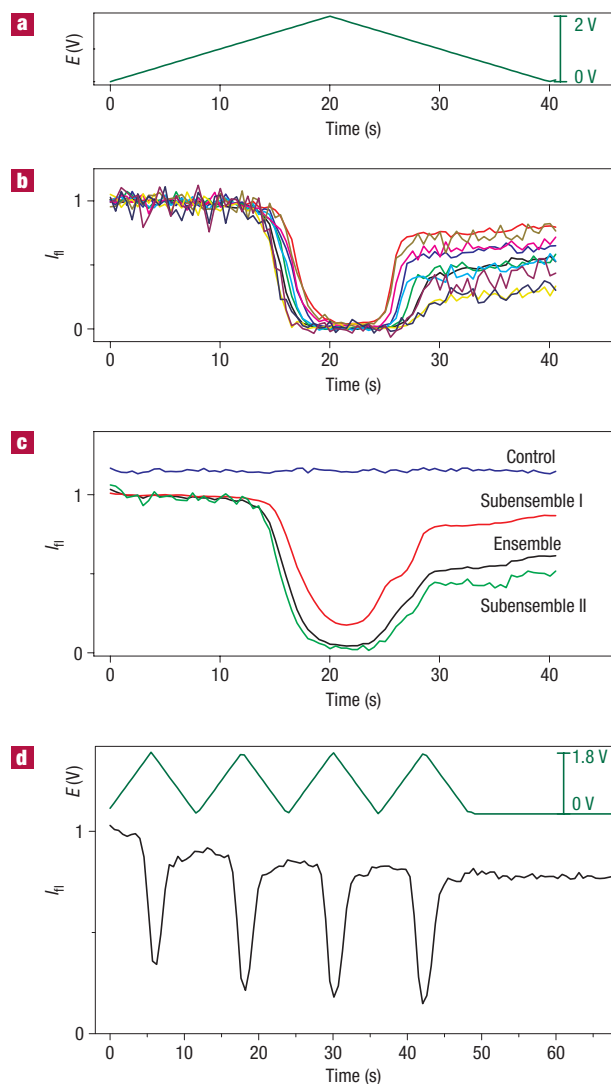


Figure 2 Single-aggregate, subensemble and ensemble SMS-EC data. **a**, Applied bias between working and reference electrodes (E). **b**, Examples of normalized single-aggregate fluorescence-intensity trajectories obtained while applying the E shown in **a** to a pristine cell. **c**, Ensemble average (50 particles) and subensembles constructed by sorting the particles on the basis of their intensities. The top 25 highest intensity particles were averaged to give subensemble I; the remaining particles were averaged to give subensemble II. The blue curve shows the total ensemble average obtained at 0 V. **d**, Total ensemble average (black curve) obtained while applying multiple potential cycles (green curve) to a pristine cell.

order of 10⁸ particles cm⁻²) compared with the experiment in Fig. 1c and the small number of electroactive nanoparticles prevents any direct measurement of the charge associated with the redox reaction of F8BT. At such a low concentration of F8BT nanoparticles, the transport of charge by a percolation process among the nanoparticles is negligible. Thus, any electron transfer between the ITO electrode and the nanoparticles must occur directly and nanoparticles that are outside the tunnelling distance are not electrochemically active. A small fraction of nanoparticles (typically <20%) exhibited no evidence of oxidation because of this effect. The intensity of the $I_{fl}(t)$ curves in Fig. 2 has been normalized to the zero bias intensity for each nanoparticle. The non-normalized intensities can vary by over a factor of 100 owing to the broad size distribution of the nanoparticles.

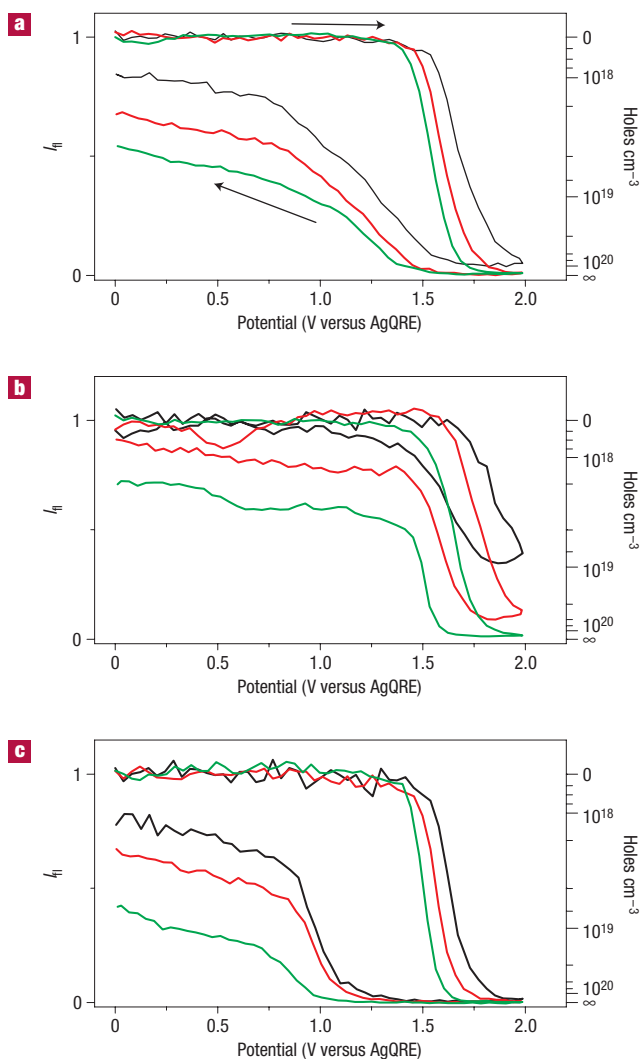


Figure 3 Dependence of single-aggregate charging/discharging behaviour on potential sweep rate. **a**, Ensemble average of normalized single-aggregate fluorescence-intensity trajectories for potential sweeping rates of 0.2 (black curve), 0.1 (red curve) and 0.05 (green curve) V s^{-1} . **b,c**, Examples of single-particle intensity trajectories as a function of sweep rate.

The shape of the fluorescence quenching curves was independent of excitation power, indicating that electrochemical oxidation of the ground state of F8BT is being monitored in this study, not the electrochemical oxidation of excited states. For the smallest particles, which can be as small as a single polymer chain, intensity fluctuations due to photochemical blinking are apparent in the data (not shown). Using the fluorescence intensity of pristine non-oxidized particles as a relative measure of particle size, we determined an effective radius for each nanoparticle. Subensemble averages of particles in a particular size range were constructed to produce higher signal-to-noise curves, as shown in Fig. 2c.

The data in Fig. 2c show that the fluorescence intensity of the nanoparticles does not completely recover after the first cycle of the electrochemical bias (even after a long rest period at 0 V (not shown)). The fractional drop in intensity after one potential cycle, f_p , is a function of particle size, with the smaller particles showing a much larger f_p . For single F8BT molecules, f_p is unity for almost every molecule after one cycle of the potential at this relatively

slow scan rate (100 mV s^{-1}), although some reversibility is seen at faster scan rates¹⁴. The lack of fluorescence intensity recovery on single molecules is attributed to a chemical reaction of oxidized F8BT, probably involving a trace amount of water in the solvent and producing some electroinactive products in the potential range studied. This side-reaction is absent when conjugated polymers are oxidized in pure bulk films or at high dilution in an inert polymer host, such as PMMA¹⁸, suggesting that the side-reaction occurs on the solvent accessible surface of the particles, but not in the ‘core’. The observation that f_p decreases as particle size is increased is also consistent with this hypothesis. Interestingly, the side-reaction is much less efficient when the nanoparticle is subjected to one or more further cycles of the potential, as shown in Fig. 2d. Apparently, the fraction of oxidizable F8BT ‘sites’ that are susceptible to the side-reaction is almost completely consumed in the first cycle of the potential. The dependence of the electrochemical behaviour on the history of potential cycling, for example, increases in the reversibility of cyclic voltammetry with the number of cycles, is frequently observed in polymer-modified electrodes and is called ‘break-in’ in the electrochemical literature⁹.

The $I_{fl}(t)$ curves in the later scans are highly reproducible from scan to scan offering the opportunity to systematically explore the charging and discharging of F8BT dynamics with a controllable potential sweep. It is useful in this regard to consider the quantitative relationship between holes(t) and $I_{fl}(t)$. The ‘quenching volume’, V_Q , for the thermalization of singlet excitons by holes in conjugated polymers is typically of the order of $\sim 200 \text{ nm}^3$ (ref. 19). For example, for single isolated F8BT molecules (molecular volume $\sim 200 \text{ nm}^3$; the molecular volume was calculated on the basis of the average molecular weight of the polymer (100 kg mol^{-1}) and assuming a density of 0.8 g ml^{-1} (typical of organic compounds)), the fluorescence quenching efficiency due to a single charge is of the order of 0.5 (ref. 17). Owing to the much larger volume of F8BT nanoparticles, V_{NP} , the efficiency of fluorescence quenching per charge (V_Q/V_{NP}) is small, for example, 0.2% for a 30 nm particle. Under these circumstances, the normalized $I_{fl}(t)$ curves should be approximately given by the well-known Stern–Volmer relationship, $I_{fl}(t) = 1/(1 + V_Q[\text{holes}(t)])$.

Using this relationship, we have constructed the approximate calibration curve that is shown in the right vertical axis of Fig. 3. Owing to a large uncertainty in both V_Q and V_{NP} , the calibration for [holes(t)] may be in error by as much as a factor of 5. This calibration indicates that the concentration of injected holes can exceed $10^{21} \text{ holes cm}^{-3}$ (1 hole nm^{-3}) in the slow scan data. This value exceeds some estimates of the maximum achievable density of holes in organic semiconductors^{3,20,21} ($\sim 10^{21} \text{ holes cm}^{-3}$). The relatively large hole density may be associated with the presence of the electrolyte in the present experiments, which should effectively screen the coulomb repulsion among the holes.

Figure 3 shows the dynamics of charging and discharging of F8BT nanoparticles during the second cycle of a linear scan of the potential. Figure 3b,c shows examples of individual fluorescence-intensity trajectories of single nanoparticles and Fig. 3a shows the ensemble average of 50 trajectories. Interestingly, during the up-sweep of the potential, charging is not detectable until the potential exceeds 1.5 V. This is consistent with the ensemble ‘true’ electrochemical measurements (Fig. 1c), which exhibit significant current flow at potentials positive of 1.4 V. The oxidation current rises rapidly above 1.5 V; however, owing to the following multiple-step electron transfer reactions, it does not reach a defined peak before the scan direction of the potential is changed. During the down-sweep of the potential, the fluorescence-intensity trajectories of individual particles (Fig. 3b,c) show fast and slow components in the fluorescence recovery. Part of the discharging process

occurs much more slowly than the injection process, and, given the coupling of potential and time during a potential sweep experiment, appears over a much larger potential range (which is also consistent with Fig. 1c).

This behaviour implies that hole injection occurs initially to shallow sites (to produce untrapped holes) but soon after injection, a small fraction of the holes are deeply trapped by either relaxation of the polymer structure (self-trapping) or by hole transfer from the initial site of hole injection to a deep-trapped hole site (another possible origin of the deep traps is the formation of a non-conductive zone between the nanoparticles and the electrode leaving a small concentration of trapped holes). The fast component of the fluorescence recovery is associated with the discharging of shallow (non-trapped) holes. The shape of the $I_h(t)$ data is qualitatively consistent with efficient trapping of the initially injected holes, implying a density for either type of hole that exceeds 10^{21} holes cm^{-3} . This suggests that deep-trapped holes are not rare defect sites, but rather are a relaxed form of the shallow traps. The deep trapping of holes in the present experiments could in principle be due to charge trapping at the nanoparticle–electrolyte interface. However, experiments using electrolytes containing large ions (see the Supplementary Information) indicate that the rate of the apparent charge trapping effect is not limited by the diffusion of electrolyte ions into polymer nanoparticles.

Figure 4 shows the fluorescent quenching electrochemical half-wave potential ($E_{1/2}$) distributions for the charging process as a function of the bias sweep rate in a sample, determined by fitting individual nanoparticles $I_h(t)$ curves to a sigmoidal function, $I_h(t)_i \approx 1/(1 + \exp((E - E_{1/2,i})/\delta E_i))$, with a variable $E_{1/2,i}$ for each particle i (ref. 14). The fitted curves are in excellent agreement with the experimental single-particle curves (see Fig. 4 insets), and the sum of the single-particle fits agrees well with the ensemble $I_h(t)$. The high reversibility at the 0.2 V s^{-1} scan rate indicates that the hole injection $E_{1/2}$ distribution in this case is close to the charging equilibrium for the untrapped holes. The narrow distribution of $E_{1/2,i}$ for each subensemble is an indication of the reliability of the use of nanoparticles for characterizing the oxidation/reduction of conjugated polymers when particles are compared within the same sample. On the other hand, we have had less reliability when comparing particles in different samples. The problem is apparently associated with good surface preparation of the ITO surface, which has a large effect on the quality of the Nafion–ITO interface. The data shown in Fig. 4 were obtained after several oxidation/reduction cycles. Measurements of $E_{1/2}$ distributions in pristine samples prepared under the same experimental conditions showed a variable proportion of two apparent $E_{1/2}$ populations peaking at ~ 1.2 and 1.7 V (not shown). Particles from both populations showed slow fluorescence recovery rates associated with the presence of deep traps. The occurrence of this apparent bimodal distribution is not currently understood.

To explore in more detail the formation and decay kinetics of deep traps, pulsed bias experiments were carried out on ‘relaxed’ nanoparticle samples (that is, after ‘break in’). Figure 5a shows the effect of applying pulses of different durations on the ensemble fluorescence intensity of many nanoparticles. An important feature to note in this figure is the increase in quenching depth with increasing pulse duration, which gives information about the kinetics of charge formation at constant bias. Following the fluorescence quenching in the forward anodic pulse, when the potential is stepped back to zero, the fluorescence is recovered at a faster initial rate (about 1.8 times the fluorescence quenching rate) followed by a much slower rate, which is not apparent by cyclic voltammetry at a scan rate of 0.1 V s^{-1} . Note that with polymer films of compounds such as polyaniline, a much slower charging process and a faster discharge process is frequently observed in

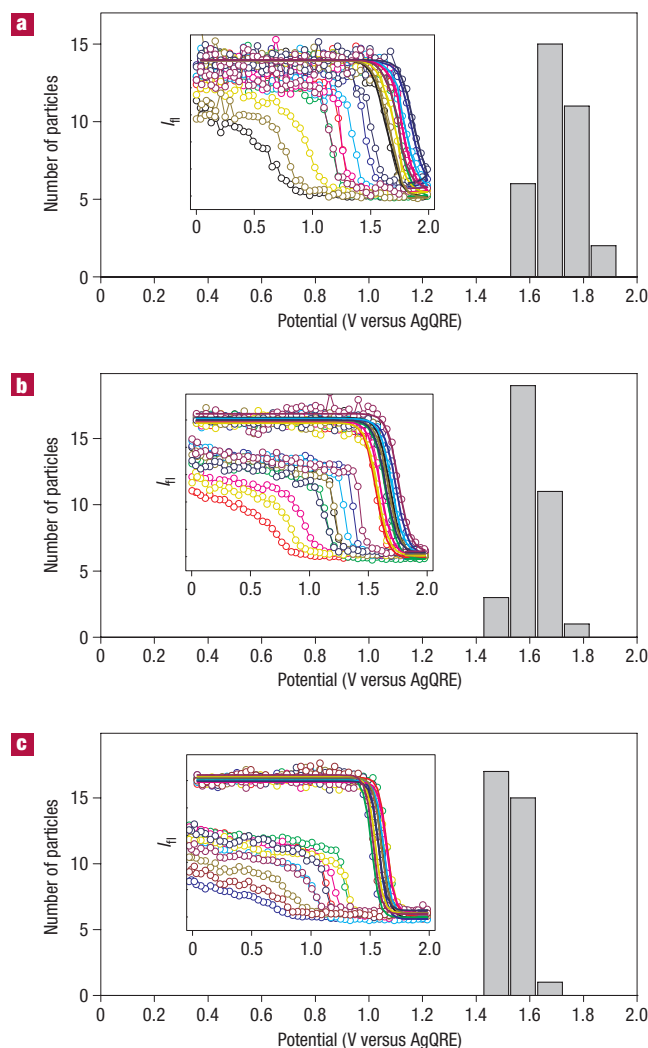


Figure 4 Dependence of $E_{1/2}$ on potential sweep rate. **a–c**, $E_{1/2}$ distributions (bars) for potential sweep rates of 0.2 (**a**), 0.1 (**b**) and 0.05 (**c**) V s^{-1} . Insets: Representative single-particle intensity trajectories (data points) and corresponding fits (smooth curves) for each potential sweep rate. Fits are used to obtain the $E_{1/2}$ for each particle.

chronoamperometry experiments¹⁰. In this case, however, much of this effect can be ascribed to differences in resistance of the uncharged and charged film. As the currents are much smaller in the SMS-EC experiments, effects of resistance should be negligible.

To further test the hypothesis of deep trap formation, we constructed a theoretical model to simulate the fluorescence intensity of nanoparticles as a function of the applied bias. The model takes into account the fluorescence quenching by initially injected and deep-trapped holes, the conversion rate of initially injected holes into deep-trapped holes and the charging/discharging dynamics of both hole species as a function of bias (see the Methods section).

As seen in Fig. 5, the simulations (blue curves) are able to reproduce the two main features associated with the presence of deep traps, that is, a decrease in intensity with increasing pulse duration (Fig. 5a) and a slow intensity recovery after oxidation (Fig. 5b). When the formation of deep traps is excluded from the model, the resulting simulations (Fig. 5, red curves) cannot reproduce these two main features. In addition, the fast

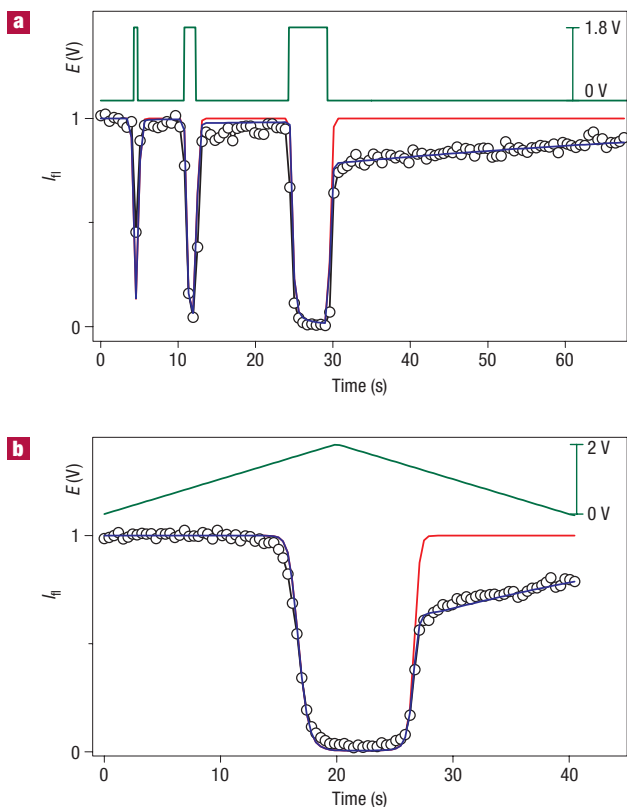


Figure 5 Pulsed bias experiments and charging/discharging simulations. **a, b**, Comparison of experimental SMS-EC data (data points) and simulations with (blue curves) and without (red curves) charge trapping (see text for details). The green curves represent the bias function applied during the experiment.

fluorescence recovery associated with the discharging of shallow holes is also well reproduced by the simulations. A detailed analysis of the ‘best-fit’ simulations indicates that the trapping rate constant is surprisingly slow ($k_T = 2 \times 10^{-3}$ (0.6×10^{-3}) s^{-1}) and only a small fraction (<1%) of the shallow traps are converted to deep traps in a typical SMS-EC experiment. Nevertheless, deeply trapped holes contribute significantly to the SMS-EC data at long times owing to the high efficiency of exciton quenching by holes.

To obtain more insight into possible reactions that follow the initial electron transfer, cyclic voltammetry studies of dissolved F8BT were carried out (see Fig. 6). At slow scan rates, for example, $\nu \leq 0.02 \text{ V s}^{-1}$, a negligibly small faradaic current (after correction for the double-layer charging) was observed on scan reversal of the forward oxidation wave and the shape of the curve is similar to that of a totally irreversible charge transfer. At higher scan rates, for example, $\nu \geq 0.1 \text{ V s}^{-1}$, some reversibility of the charge transfer was observed. Detailed analyses suggest an electrochemical reaction scheme that involves two parallel reactions: a pseudo first-order reaction to produce an electroinactive product P ($k_{f,2} = 2.5 \text{ s}^{-1}$; $k_{b,2} < 0.01 \text{ s}^{-1}$) and dimerization ($k_{f,3} = 5,000 \text{ M}^{-1} \text{ s}^{-1}$; $k_{b,3} = 0.01 \text{ M}^{-1} \text{ s}^{-1}$) following the initial electron transfer ($k_{s,1} = 0.0005 \text{ cm s}^{-1}$) (see the Supplementary Information). Here, k_s is the heterogeneous rate constant, k_f is the rate constant of the forward chemical reaction and k_b is the rate constants of its reverse reaction.

Although the solution-phase chemistry only distantly relates to the behaviour of nanoparticles, it suggests that there may be several trapped states of the hole, for example, the species we denote P that might recover only slowly to the parent state.

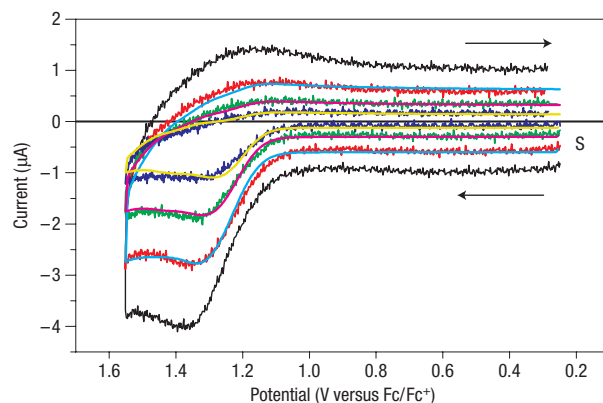


Figure 6 Solution-phase cyclic voltammograms of F8BT at different potential scan rates. Experimental curves: dark blue (0.02 V s^{-1}), green (0.05 V s^{-1}), red (0.1 V s^{-1}) and black (0.2 V s^{-1}). Simulated curves: yellow (0.02 V s^{-1}), violet (0.05 V s^{-1}) and light blue (0.1 V s^{-1}). For simulation, the solution resistance was taken as $1 \text{ k}\Omega$ and double-layer capacitance as $6 \mu\text{F}$. Point S represents the starting point of the potential scan and arrows represent the scan directions.

METHODS

SMS-EC SET-UP

The SMS-EC cells used in these experiments (Fig. 1a) comprised a planar transparent ITO working electrode, a planar gold counter electrode and a silver wire quasireference electrode (AgQRE), which was inserted in the gap between the two planar electrodes¹⁴. The AgQRE potentials were observed to be $0.20 \pm 0.05 \text{ V}$ more negative than the (Fc/Fc⁺) couple internal standard that was introduced into the cell after the SMS-EC data were acquired. The ITO electrode was spin-coated with a 20–60-nm-thick Nafion layer embedded with F8BT nanoparticles ($0.1\text{--}1 \text{ particles } \mu\text{m}^{-2}$). The gap between the planar electrodes was filled with an acetonitrile solution containing 0.2 M supporting electrolyte, LiClO₄. The time dependence of the fluorescence intensity of individual fluorescence ‘spots’, each due to a single F8BT nanoparticle, was determined from a set of images (Fig. 1b) that were recorded by a wide-field microscope (Eclipse TE2000, ‘Nikon’; ‘Roper Scientific’, Cascade 512B, CCD camera) using 488 nm excitation (total internal reflectance fluorescence).

The SMS-EC cells studied here are assembled in a non-controlled environment. Experiments carried out in a controlled environment (see the Supplementary Information) show that the slow component of the fluorescence recovery is still observed in water- and oxygen-depleted conditions (see Supplementary Information, Fig. S4). These results are qualitatively similar to those from experiments carried out in ambient conditions, suggesting that water and oxygen do not play a significant role in the observed slow fluorescence recovery phenomena.

For both the linearly scanned and pulsed SMS-EC experiments, the timing of the collection of the fluorescence images was synchronized with the time-varying electrochemical potential, $E(t)$, of the working electrode. $E(t)$ was maintained at the required potential relative to the reference electrode (AgQRE) by a potentiostat (PGSTAT 100, ‘Autolab’).

Aggregates were prepared by the reprecipitation technique^{11,12}. In brief, $100 \mu\text{l}$ of a $\sim 5 \text{ mg ml}^{-1}$ F8BT/tetrahydrofuran solution is ‘flash’-injected into 10 ml of deionized water and the resulting colloidal suspension is filtered through a membrane filter (pore size $200 \mu\text{m}$). A small aliquot of the suspension is added to a 2% Nafion solution and spin-cast at $2,000 \text{ r.p.m.}$ to form the SMS-EC films. On the basis of fluorescence intensity comparisons with single molecules, the radii of the aggregates are in the $5\text{--}30 \text{ nm}$ range ($10\text{--}600$ polymer chains), in good agreement with atomic force microscopy measurements¹¹.

MODEL FOR THE FLORESCENCE QUENCHING OF NANOPARTICLES

The model is based on the presence of two types of site for holes: shallow and deep. Reduced (neutral) shallow sites (S) are electrochemically oxidized to give shallow holes (S⁺) (equation (1)) that can relax to give deep holes (D⁺) with a

rate constant k_T (equation (2)). Deep holes are reduced to form empty deep sites (D) (equation (3)) that can also relax to give reduced shallow sites (S) with a rate constant k_T (equation (4)). The total number of sites per particle is given by N (equation (5)). The rate for oxidation and reduction of shallow and deep sites was calculated as a function of the applied bias using the Marcus theory to estimate the rate constants for the heterogeneous electron transfer in equations (1) and (3). It was assumed that all of the shallow and deep sites had identical $E_{1/2}$ values, $E_{1/2,S}$ and $E_{1/2,D}$, respectively.



$$N = [S] + [S^+] + [D] + [D^+] \quad (5)$$

The concentrations of oxidized/reduced deep and shallow sites as a function of time (bias) were obtained by solving the corresponding differential equations and the normalized fluorescence intensity was calculated using equation (6) (ref. 18).

$$\frac{I(E)}{I(0)} = \frac{([S] + [D])}{N} \left[1 + \frac{QD}{1 - QD} ([S^+] + [D^+]) \right]^{-1} \quad (6)$$

where $([S] + [D])$ and $([S^+] + [D^+])$ are the total number of sites in reduced and oxidized states, respectively, and QD is the normalized fluorescence quenching depth per oxidized site (assumed the same for S^+ and D^+). The Marcus electrochemical calculation used the same reorganization energy, λ , for both types of site and different pre-exponential factors, $k_{0,S}$ and $k_{0,D}$, for shallow and deep sites respectively. Some of the parameters used in the simulations shown in Fig. 5a,b were values based on previous results, that is, $N = 1.5 \times 10^4$ (10^4), $\lambda = 0.5$ (0.5) eV, $QD^{19} = 0.02$ (0.02). Others were determined by trial-and-error fitting of the simulation to experiment, that is, $E_{1/2,S} = 1.80$ (1.73) eV, $E_{1/2,D} = 1.40$ (1.40) eV, $k_{0,S} = 7$ (5) s^{-1} , $k_{0,D} = 0.02$ (0.06) s^{-1} and $k_T = 2 \times 10^{-3}$ (0.6×10^{-3}) s^{-1} .

BULK ELECTROCHEMISTRY

F8BT in Nafion thin films for cyclic voltammetry were cast from a mixed solution (1:1 by volume) of 1% Li^+ -Nafion in methanol and F8BT in benzene (1.66 mg ml^{-1}). Solution-phase electrochemistry at a glassy carbon electrode was carried out by dissolving F8BT (~ 0.5 mM in terms of monomer) in an acetonitrile:benzene (1:6 by volume) mixed solvent containing 0.2 M of $TBAPF_4$ as the supporting electrolyte. Detailed analyses of the data and simulation of the cyclic voltammograms were carried out with the DigiElch software package^{22–27}.

Received 9 October 2006; accepted 21 June 2007; published 22 July 2007.

References

- Campbell, A. J., Bradley, D. D. C. & Antoniadis, H. Dispersive electron transport in an electroluminescent polyfluorene copolymer measured by the current integration time-of-flight method. *Appl. Phys. Lett.* **79**, 2133–2135 (2001).
- Chang, J. B. & Subramanian, V. Effect of active layer thickness on bias stress effect in pentacene thin-film transistors. *Appl. Phys. Lett.* **88**, 233513 (2006).

- Gomes, H. L. *et al.* Bias-induced threshold voltages shifts in thin-film organic transistors. *Appl. Phys. Lett.* **84**, 3184–3186 (2004).
- Lang, D. V., Chi, X., Siegrist, T., Sergeant, A. M. & Ramirez, A. P. Bias-dependent generation and quenching of defects in pentacene. *Phys. Rev. Lett.* **93**, 076601 (2004).
- Matters, M., De Leeuw, D. M., Herwig, P. T. & Brown, A. R. Bias-stress induced instability of organic thin film transistors. *Synth. Met.* **102**, 998–999 (1999).
- Salleo, A. & Street, R. A. Light-induced bias stress reversal in polyfluorene thin-film transistors. *J. Appl. Phys.* **94**, 471–479 (2003).
- Seceley, A. J. A. B., Friend, R. H., Kim, J.-S. & Burroughes, J. H. Trap-assisted hole injection and quantum efficiency enhancement in poly(9,9'-dioctylfluorene-alt-benzothiadiazole) polymer light-emitting diodes. *J. Appl. Phys.* **96**, 7643–7649 (2004).
- Muller, E. M. & Marohn, J. A. Microscopic evidence for spatially inhomogeneous charge trapping in pentacene. *Adv. Mater.* **17**, 1410–1414 (2005).
- Inzelt, G. Mechanism of charge transport in polymer-modified electrodes. *Electroanal. Chem.* **18**, 89–241 (1994).
- Bard, A. J. & Faulkner, L. R. *Electrochemical Methods: Fundamentals and Applications* (Wiley, New York, 2001).
- Grey, J. K., Kim, D. Y., Norris, B. C., Miller, W. L. & Barbara, P. F. Size dependent spectroscopic properties of conjugated polymer nanoparticles. *J. Phys. Chem. B* **110**, 25568–25572 (2006).
- Szymanski, C. *et al.* Single molecule nanoparticles of the conjugated polymer MEH-PPV, preparation and characterization by near-field scanning optical microscopy. *J. Phys. Chem. B* **109**, 8543–8546 (2005).
- Halls, J. J. M. *et al.* Photodiodes based on polyfluorene composites: Influence of morphology. *Adv. Mater.* **12**, 498–502 (2000).
- Palacios, R. E., Fan, F.-R. F., Bard, A. J. & Barbara, P. F. Single-molecule spectroelectrochemistry (SMS-EC). *J. Am. Chem. Soc.* **128**, 9028–9029 (2006).
- Barbara, P. F., Gesquiere, A. J., Park, S.-J. & Lee, Y. J. Single-molecule spectroscopy of conjugated polymers. *Acc. Chem. Res.* **38**, 602–610 (2005).
- Grey, J. K. *et al.* Effect of temperature and chain length on the bimodal emission properties of single polyfluorene copolymer molecules. *J. Phys. Chem. B* **110**, 18898–18903 (2006).
- Lammi, R. K. & Barbara, P. F. Influence of chain length on exciton migration to low-energy sites in single fluorene copolymers. *Photochem. Photobiol. Sci.* **4**, 95–99 (2005).
- Gesquiere, A. J., Park, S.-J. & Barbara, P. F. F-V/SMS: A new technique for studying the structure and dynamics of single molecules and nanoparticles. *J. Phys. Chem. B* **108**, 10301–10308 (2004).
- Yu, J., Song, N. W., McNeill, J. D. & Barbara, P. F. Efficient exciton quenching by hole polarons in the conjugated polymer MEH-PPV. *Isr. J. Chem.* **44**, 127–132 (2004).
- Arkhipov, V. I., Heremans, P., Emelianova, E. V. & Bassler, H. Effect of doping on the density-of-states distribution and carrier hopping in disordered organic semiconductors. *Phys. Rev. B* **71**, 045214 (2005).
- David, P. S., Campbell, I. H. & Smith, D. L. Device model for single carrier organic diodes. *J. Appl. Phys.* **82**, 6319–6325 (1997).
- Rudolph, M. Reply to L. K. Bieniasz's comments on my paper Digital simulations on unequally spaced grids. Part 1. Critical remarks on using the point method by discretisation on transformed grid [J. Electroanal. Chem. 529 (2002) 97]. *J. Electroanal. Chem.* **558**, 171–176 (2003).
- Rudolph, M. Digital simulations on unequally spaced grids. Part 2. Using the box method by discretization on a transformed equally spaced grid. *J. Electroanal. Chem.* **543**, 23–39 (2003).
- Rudolph, M. Digital simulations on unequally spaced grids. Part 3. Attaining exponential convergence for the discretisation error of the flux as a new strategy in digital simulations of electrochemical experiments. *J. Electroanal. Chem.* **571**, 289–307 (2004).
- Rudolph, M. Attaining exponential convergence for the flux error with second- and fourth-order accurate finite-difference equations. Part 3. Application to electrochemical systems comprising second-order chemical reactions. *J. Comput. Chem.* **26**, 1193–1204 (2005).
- Rudolph, M. Attaining exponential convergence for the flux error with second- and fourth-order accurate finite-difference equations. II. Application to systems comprising first-order chemical reactions. *J. Comput. Chem.* **26**, 633–641 (2005).
- Rudolph, M. Attaining exponential convergence for the flux error with second- and fourth-order accurate finite-difference equations. I. Presentation of the basic concept and application to a pure diffusion system. *J. Comput. Chem.* **26**, 619–632 (2005).

Acknowledgements

This work was supported by the National Science Foundation, AFOSR, the Welch Foundation (P.F.B. and A.J.B.) and by the Basic Energy Sciences Program of the Department of Energy (P.F.B.). Correspondence and requests for materials should be addressed to P.F.B. Supplementary Information accompanies this paper on www.nature.com/naturematerials.

Author contributions

R.E.P. and F.R.F.F. were primarily responsible for instrumental set-up, sample preparation and data acquisition. J.K.G. and J.S. were involved in the instrumental set-up for the controlled-environment SMS-EC experiments. R.E.P., F.R.F.F., A.J.B. and P.F.B. were responsible for project planning, experiment design, data analysis and interpretation and manuscript preparation.

Competing financial interests

The authors declare no competing financial interests.

Reprints and permission information is available online at <http://npg.nature.com/reprintsandpermissions/>